

# Three-body decay of the $d^*$ dibaryon

Chun Wa WONG

*Department of Physics and Astronomy, University of California, Los Angeles, CA 90095-1547*

(February 9, 2008)

Under certain circumstances, a three-body decay width can be approximated by an integral involving a product of two off-shell two-body decay widths. This “angle-average” approximation is used to calculate the  $\pi NN$  decay width of the  $d^*(J^\pi = 3^+, T = 0)$  dibaryon in a simple  $\Delta^2$  model for the most important Feynman diagrams describing pion emissions with baryon-baryon recoil and meson retardation. The decay width is found to be about 0.006 (0.07, 0.5) MeV at the  $d^*$  mass of 2065 (2100, 2150) MeV for input dynamics derived from the Full Bonn potential. The smallness of this width is qualitatively understood as the result of the three-body decay being “third forbidden”. The concept of  $\ell$  forbiddenness and the threshold behavior of a three-body decay are further studied in connection with the  $\pi NN$  decay of the dibaryon  $d'(J^\pi = 0^-, T = 0 \text{ or } 2)$  where the idea of unfavorability has to be introduced. The implications of these results are briefly discussed.

PACS number(s):

## I. INTRODUCTION

Almost all theoretical dibaryons with exotic quark structures have masses above the  $\pi NN$  threshold [1]. They can thus decay into  $\pi NN$  states. From the viewpoint of dibaryon searches, the most promising candidates should have the narrowest widths, otherwise they do not stand out clearly above the background. However, their  $\pi NN$  widths should not be too small, otherwise too few pions will be available to help with the identification. Hence a qualitative understanding of the  $\pi NN$  decays of these dibaryons is of considerable interest when contemplating an experimental search for these dibaryons.

A particularly interesting dibaryon is the  $d^*$ , of quantum numbers  $J^\pi T = 3^+ 0$ . The interest comes from the possibility that its mass might be unusually low, thereby indicating an unusual structure or dynamics [2–4]. The purpose of this paper is to give rough estimates of its  $\pi NN$  decay width when it is treated approximately as an S-wave bound  $\Delta\Delta$  state of intrinsic spin  $S = 3$ .

The  $\pi NN$  decay of this model  $d^*$  cannot occur via pion emission from one of the constituent  $\Delta$ 's because the spectator baryon will remain a  $\Delta$ . Hence the baryons must interact at least once to turn the spectator into a final-state nucleon. This is true too for pion emission from a virtual meson which must be made to appear in the system. With one pion emission vertex and two interaction vertices for the spectator interaction (referred to below as a recoil), the leading Feynman diagrams are processes containing three vertices, as shown in Figs. 1 and 2.

Of the processes shown, Fig. 1a-c are recoil diagrams describing  $\pi$  emission by interacting baryons. Fig. 1d-f are retardation diagrams describing emission from a baryon when a virtual meson is in the air. Figs. 1g-i are some of the relativistic corrections coming from  $NN$  pairs. Finally Fig. 2 gives the contributions for emission from an exchanged meson itself. We shall calculate the decay width for the most important of these processes

with the help of an approximate angle-average formula developed in this paper.

This paper is organized as follows: The general nature of the  $\pi NN$  decay of the model  $d^*$  is described in Sec. II for P- and S-wave pion emissions. The concept of  $\ell$ -forbiddenness for describing the threshold behavior of three-body decays is introduced in analogy to that for nuclear  $\beta$  decays. Both P-wave and S-wave pion emissions from baryons described by Fig. 1 are found to be “third-forbidden”. The processes shown in Fig. 2 for pion emission from virtual mesons in the leading order are found to vanish for both P-wave and S-wave pion emissions.

In Sec. III, an angle-average approximation for the width of a three-body decay of the type shown in Fig. 1 is obtained in the form of a sum of integrals over the product of two sets of off-shell two-body decay amplitudes. Numerical results are given in Sec. IV where this angle-average approximation is applied to Figs. 1a-c, using baryon dynamics derived from the Full Bonn potential [5] and from on-shell  $NN$   $t$ -matrices constructed from experimental  $NN$  phase shifts [6]. In Sec. V, retardation and pair contributions are included as well.

Sec. VI gives a discussion of the threshold behaviors of  $\pi NN$  decays, which are controlled but not solely determined by the  $\ell$ -forbiddenness of the decay. The decay of the  $d'(J^\pi = 0^-, T = 0 \text{ or } 2)$  dibaryon is studied to illustrate the complications caused by decays with abnormally large power dependences on the external momenta near threshold.

Finally, brief concluding remarks are made in Sec. VII, where the implications of our results for the quark-delocalization model of  $d^*$  [2–4] are touched upon. In particular, the calculated decay width of 70 keV at  $m^* = 2100$  MeV seems to imply that there might be too few decay pions at low dibaryon masses to help with particle identification.

## II. GENERAL CONSIDERATIONS

The dibaryon  $d^*$  is an isoscalar, high-spin ( $J^\pi = 3^+$ ) state. When treated as a  $\Delta^2$  bound state, its dominant spatial component is  ${}^7S_3$ . Fig. 1 gives the lowest-order Feynman diagrams for its decay into the  $\pi NN$  final state by pion emission from a baryon. For P-wave pion emission, the  $NN$  system in the  $\pi NN$  final state has  $ST = 01$ , the possible partial waves being  ${}^1D_2$  and  ${}^1G_4$ . Hence the  $\pi NN$  decay of  $d^*$  through this dominant  ${}^7S_3$  component requires three units of baryon spin change, i.e. a rank-3 intrinsic spin tensor.

This rank-3 spin tensor must be combined into a rotational scalar as the perturbation responsible for the decay by scalar multiplication with a rank-3 spatial tensor made up of internal or external momenta. The Feynman diagrams shown in Fig. 1 describe some of the leading-order pion emission by a baryon in our simple model of  $d^*$ . The dominant process involves a P-wave pion emission that depends linearly on the momentum  $\mathbf{p}_3 = \mathbf{p}_\pi$  of the emitted pion. This means that the remaining  $qq$  or  $BB$  interaction must generate a rank-two spatial tensor to trigger the decay. This cannot be done with a rank-0 central interaction, or a rank-1 spin-orbit interaction. A rank-2 tensor-force interaction is needed. Furthermore, the final  $NN$  state with the lowest orbital angular momentum that appears from the initial dominant spatial  ${}^7S_3$ -state of  $d^*$  is  ${}^1D_2$ .

To the extent that  $d^*$  is dominated by the  $\Delta^2$  component containing two  $t = 3/2$  constituents, the tensor interaction for recoil must convert at least one of these constituents into a  $t = 1/2$  nucleon. Thus the tensor force must be an isovector interaction that arises, for example, from the exchange of an isovector meson such as  $\pi$  or  $\rho$ . This means that the operator in the  $BB$  interaction responsible for the decay in our simple  $\Delta^2$  model of  $d^*$  is  $(\boldsymbol{\sigma}_i \times \boldsymbol{\sigma}_j)^{(2)}(\boldsymbol{\tau}_i \cdot \boldsymbol{\tau}_j)$ , where  $i$  and  $j$  refer to two separate baryons, or to quarks in these baryons. The operators  $\boldsymbol{\sigma}$  and  $\boldsymbol{\tau}$  are Pauli spin operators for quarks, and generalized spin operators for baryons [7].

It is useful to enumerate the possible components of both the initial  $d^*$  and the  $B^2$  states appearing after P- or S-wave pion emission. We shall use a baryon notation with baryon components restricted to only  $\Delta$  and  $N$  because these baryons have the lowest masses and the same spatial  $s^3$  quark structure. They can therefore be expected to mix strongly with one another. Under the circumstances, the available states are

$$\begin{aligned} d^*(J^\pi = 3^+, T = 0) : & \Delta^2[{}^7(S, D, G, I)]; \\ & N^2[{}^3(D, G)]; \\ B^2(J^\pi = 2^+/4^+, T = 1) : & N^2[{}^1(D, G)]; \\ & \Delta N[{}^5(S, D, G, I)], [{}^3(D, G)]; \\ & \Delta^2[{}^5(S, D, G, I)], [{}^1(D, G)]; \\ B^2(J^\pi = 3^-, T = 1) : & N^2[{}^3F]; \end{aligned}$$

$$\begin{aligned} & \Delta N[{}^5(P, F, H)], [{}^3(P, F)]; \\ & \Delta^2[{}^7(P, F, H)], [{}^3(P, F)]. \end{aligned} \quad (1)$$

The decay processes shown in Figs. 1a-c can then be described by certain decay equations. For P-wave emission, they are

$$\begin{aligned} \Delta^2({}^7S_3) & \rightarrow N^2({}^3D_3) \rightarrow N^2({}^1D_2) + \pi(\ell_\pi = 1); \\ \Delta^2({}^7S_3) & \rightarrow \Delta N({}^5S_2) + \pi(\ell_\pi = 1), \\ & \Delta N({}^5S_2) \rightarrow N^2({}^1D_2); \\ \Delta^2({}^7S_3) & \rightarrow \Delta^2({}^5S_2) + \pi(\ell_\pi = 1), \\ & \Delta^2({}^5S_2) \rightarrow N^2({}^1D_2). \end{aligned} \quad (2)$$

In this paper, we are particularly interested in low-mass dibaryons decaying close to its  $\pi NN$  threshold. Such near-threshold decays show certain general kinematical features reminiscent of nuclear  $\beta$  decays, features that originate from the dominance of centrifugal potential barriers on the outgoing decay products, and are controlled by their orbital angular momenta. The transition amplitude can be expanded in a Taylor series in these final-state momenta of which only two, say  $\mathbf{p}_\pi$  of the pion and  $\mathbf{p}_N$  of one of the nucleons, are independent. If  $\ell_\pi$  is the pion orbital angular momentum in the dibaryon c.m. frame, and  $\ell_N$  is the relative orbital angular momentum of the  $NN$  system in the final state, the leading terms in the Taylor expansion are necessarily of the type  $\mathcal{Y}_{\ell_\pi m_\pi}(\mathbf{p}_\pi)\mathcal{Y}_{\ell_N m_N}(\mathbf{p}_N)$ , where  $\mathcal{Y}_{\ell m}(\mathbf{p})$  is a solid spherical harmonic. The decay width near threshold is then proportional to  $(p_\pi^{\ell_\pi} p_N^{\ell_N})^2$  together with additional factors coming from the three-body phase space which we shall find in Sec. VI to be  $p_\pi^2 p_N^2$ . We shall call this decay  $\ell$ -forbidden when  $\ell = \ell_\pi + \ell_N$  is nonzero. With  $\ell_\pi = 1$  and  $\ell_N = 2$ , the P-wave pion decays of Eq. (2) are all third-forbidden.

This concept of  $\ell$ -forbiddenness is familiar not only from nuclear  $\beta$  decays, but also from the simpler processes of two-body decays. For example, the decay of the  $\Delta$  resonance involves P-wave pion emission, of  $\ell_\pi = 1$ . Hence the decay is  $\ell = 1$  forbidden in our language. The two-body phase space gives an additional factor of  $p_\pi$ . The decay width is then roughly proportional to  $p_\pi^3$ . This is a well-known result.

The  $\ell$ -forbiddenness of the decay  $d^* \rightarrow \pi NN$  is determined as follows: The pion has both orbital and total angular momenta  $\ell_\pi$ , and parity  $\pi_\pi = (-1)^{\ell_\pi+1}$ . The initial state has quantum numbers  $J_i^\pi = 3^+, T = 0$ . Hence the quantum numbers of the most favorable final  $NN$  state is  $T = 1$ ,  $\ell_N = |J_i - \ell_\pi|$ , and  $\pi_N = \pi_i \pi_\pi$ . From these selection rules, we can determine that the decay  $d^* \rightarrow \pi NN$  is  $\ell = J_i = 3$  forbidden for  $\ell_\pi = 0 - 3$ . For higher  $\ell_\pi > J_i$ , it is  $\ell = 2\ell_\pi - J_i$  forbidden.

These selection rules for  $\pi NN$  decays have been specified in terms of the relative coordinate of the final  $NN$  state, i.e. a Jacobi coordinate. This is the most natural choice because wave-function antisymmetrization and

final-state interactions can then be described most conveniently. However, it is not the only one possible. Selection rules can also be specified in terms of the one of the final-state nucleon coordinates. This choice could occasionally be more convenient, for example when the nucleon is a real spectator. An example of this choice will be given in Sec. VI.

Let us now return to the decay of  $d^*$ . For S-wave pion emissions, the final  $NN$  system should have odd spatial parity, and therefore  $ST = 11$ . Only one  $N^2$  partial wave is then possible, namely  ${}^3F_3$ . Figs. 1a-c for S-wave pion emission from a baryon are described by the decays

$$\begin{aligned}\Delta^2({}^7S_3) &\rightarrow N^2({}^3D_3) \rightarrow N^2({}^3F_3) + \pi(\ell_\pi = 0); \\ \Delta^2({}^7S_3) &\rightarrow \Delta N({}^5P_3) + \pi(\ell_\pi = 0), \\ &\Delta N({}^5P_3) \rightarrow N^2({}^3F_3), \\ \Delta^2({}^7S_3) &\rightarrow \Delta^2({}^7P_3) + \pi(\ell_\pi = 0), \\ &\Delta^2({}^7P_3) \rightarrow N^2({}^3F_3),\end{aligned}\quad (3)$$

respectively. Like P-wave pion-emission amplitudes, the S-wave amplitudes interfere among themselves, but they add only incoherently to the P-wave contributions to the decay width.

Now the basic S-wave pion emission vertex is known [8] to be of order  $w/m$  relative to P-wave pion emission, where the baryon (or quark) energy transfer  $w = E - E'$  is expected to be significantly smaller than the baryon mass  $m$  for low-mass  $d^*$ . Given the fact that these S-wave decays are also  $\ell = 3$  forbidden, we conclude that they can be neglected in comparison with P-wave emissions, at least for the rough estimates attempted in this paper.

Other types of S-wave pion emission are possible if the Feynman diagrams involve orbitally or radially excited baryons  $\Delta^*$  or  $N^*$  as well. These additional baryon configurations can be expected to be even less important because the  $mBB^*$  coupling constants are much smaller than the meson coupling constants to  $\Delta$  or  $N$  because of the spatial quark excitations.

Among higher-order diagrams not included in Fig. 1 are those describing final-state interactions between the outgoing nucleons. They are not expected to be very important because the nucleons have large relative orbital angular momenta in our final states. Thus re-scattering effects in  $d^* \rightarrow \pi NN$  decays could be quite different from those of threshold pion production in nuclear reactions [9,10].

Let us turn next to Fig. 2 describing pion emission from virtual  $\pi - \rho$  mesons. The operators involved in Fig. 2a have been derived in connection with the study of  $\pi\pi\rho$ -exchange three-nucleon forces [11]. Two pion-emission operators appear: The first is  $(\boldsymbol{\sigma}_2 \cdot \mathbf{q})(\boldsymbol{\tau}_2 \times \boldsymbol{\tau}_1) \cdot \boldsymbol{\Phi}$ , where  $\mathbf{q}$  is the momentum of the virtual pion and  $\boldsymbol{\Phi}$  is its wave function. The spin-isospin operators appearing here could be those of quarks or of baryons (including transition spins) depending on the dynamical model used.

For simplicity, however, we shall visualize them in this section as generalized baryon spin operators.

This pion-emission operator describes S-wave pion emission. For the two diagrams in Fig. 2 together, S-wave pion emission involves the combination  $(\boldsymbol{\sigma}_1 + \boldsymbol{\sigma}_2) \cdot \mathbf{q}(\boldsymbol{\tau}_1 \times \boldsymbol{\tau}_2) \cdot \boldsymbol{\Phi}$ . This is a rank-1 spin operator. Hence the direct decay of the major component  $\Delta^2({}^7S_3)$  of  $d^*$  (i.e. Fig. 2) to the only available  $N^2$  final state of  ${}^3F_3$  is not possible. The process has to go through a minor component of either  $d^*$  or the final  $B^2$  state. A minor component of the final  $B^2$  state is one which contains one or more  $\Delta$ 's that must be converted to nucleons before the decay is completed.

The second operator appearing in Fig. 2a is proportional to  $(\boldsymbol{\sigma}_2 \cdot \mathbf{q})\boldsymbol{\sigma}_1 \cdot (\mathbf{p}_3 \times \mathbf{q})(\boldsymbol{\tau}_2 \times \boldsymbol{\tau}_1) \cdot \boldsymbol{\Phi}$ , obtainable also from  $\pi\pi\rho$ -exchange three-nucleon forces. It gives rise to a pion emission operator of the form  $-2(\boldsymbol{\sigma}_1 \times \boldsymbol{\sigma}_2) \cdot [\mathbf{q} \times (\mathbf{p}_3 \times \mathbf{q})](\boldsymbol{\tau}_1 \times \boldsymbol{\tau}_2) \cdot \boldsymbol{\Phi}$ , describing P-wave pion emission. The intrinsic spin operator appearing in it is also only rank 1. It too cannot connect the dominant  $\Delta^2({}^7S_3)$  component of  $d^*$  to the available  $N^2$  final states  ${}^1D_2$  or  ${}^1G_4$ . Hence P-wave pion emission by a virtual meson is again possible only through a minor component in the initial or the final state.

To summarize, to the lowest order in the strong-interaction vertices, the decay  $d^* \rightarrow \pi NN$  involves the processes described by Fig. 1 involving pion emissions from baryons.

### III. ANGLE-AVERAGE APPROXIMATION FOR THREE-BODY DECAY WIDTHS

Estimates of the width of a three-body decay of the type shown in Fig. 1 are greatly facilitated by using an angle-average approximation developed in this section.

We begin by noting that Fig. 1a can be interpreted as the off-shell decay  $N \rightarrow \pi N$  of a small  $NN({}^3D_3)$  component of  $d^*$  that has one spectator nucleon on its energy shell. This component is generated perturbatively by the recoil interaction from the  $\Delta^2({}^7S_3)$  state. For this reason, the energy denominator that appears is the bound-state expression

$$D_a = m^* - 2E(\mathbf{p}_2), \quad (4)$$

where  $m^*$  is the  $d^*$  mass and  $E$  is a nucleon energy in the  $d^*$  c.m. frame. The  $t$ -matrix appearing in the recoil interaction is an off-shell  $t$ -matrix between two baryons calculated at the initial-state energy  $\sqrt{s} = m^*$ .

On the other hand, Figs. 1b and c involve pion emission into abnormal or minor  $\Delta^2$  or  $\Delta N$  components of the final  $B^2$  channels. These abnormal components are off-shell with finite spatial extensions when the available energy is below their breakup threshold.

Figs. 1b and c are also similar in that their energy denominators are scattering-state quantities of the type

$$D_b = E(\mathbf{p}_1) + E(\mathbf{p}_2) - E_\Delta(-\mathbf{p}) - E(\mathbf{p} - \mathbf{p}_3), \quad (5)$$

$$D_c = E(\mathbf{p}_1) + E(\mathbf{p}_2) - E_\Delta(-\mathbf{p}) - E_\Delta(\mathbf{p} - \mathbf{p}_3), \quad (6)$$

where  $E_\Delta$  is a  $\Delta$  energy in the  $d^*$  c.m. frame. Neither energy denominator vanishes below the appropriate threshold. The off-shell  $BB$   $t$ -matrix is that calculated at the energy of the final-state  $NN$  pair.

The  $n$ -body decay of an object of mass  $m^*$  can be expressed conveniently by the Fermi golden rule [12]:

$$\Gamma = (2\pi) \int \left( \frac{1}{dE} \right) \prod_{i=2}^n \left[ \frac{d^3\mathbf{p}}{(2\pi)^3} \right]_i \langle |H'_{\text{fi}}|^2 \rangle_{\text{spin}} \times \delta(m^* - E) dE, \quad (7)$$

where  $H'$  is the effective perturbing Hamiltonian. The  $n$ -body density of states that appears can be expressed nominally in terms of a product of densities of states of fewer bodies. If the spin-average squared matrix element  $\langle |H'_{\text{fi}}|^2 \rangle_{\text{spin}}$  is also factorable into appropriate factors referring to fewer bodies in the problem, the integral could be simplified to make the physics more transparent.

To study this possibility for  $d^*$ , we first note that each Feynman diagram of Fig. 1 has the simple form of  $H_2 D^{-1} H_3$ , where  $H_i$  is one of the interactions and  $D$  is the energy denominator between them. The three-body phase space is unfortunately made complicated by the requirement of energy conservation which leaves behind the integrations over

$$\left( \frac{1}{dE_1} \right) \prod_{i=2}^3 d^3\mathbf{p}_i = E_1 E_2 E_3 dE_2 dE_3 d^2\Omega_3 d\phi_{23}. \quad (8)$$

Here use has been made of the momentum-conserving relation

$$E_1^2 = p_2^2 + p_3^2 + 2p_2 p_3 \cos \theta_{23} + m_1^2 \quad (9)$$

in the form

$$\frac{d \cos \theta_{23}}{dE_1} = \frac{E_1}{p_2 p_3}. \quad (10)$$

Thus only one set of angle integrations, here  $d^2\Omega_3$ , is formally identical to that for the decay in free space.

What is left of the second set of angle integrations, namely  $d\phi_{23}$ , has been partly changed by the requirement of energy-momentum conservation for all three particles. As a result, kinematical quantities such as  $E_1$  and  $\theta_{23}$  are no longer independent of each other. Many of the angular functions in the integrand become quite complicated. The energy denominator  $D$  too could be a function of some of these angle variables.

We are interested here in an angle-average approximation obtained by adding an extra angle integration  $(1/2)d \cos \theta_{23}$  to Eq. (8) to restore the full angle integration of  $d^2\Omega_2$ . The idea is to undo the angular correlation

between the matrix elements of the interactions  $H_1$  and  $H_2$  (so that the the angle integrations  $d^2\hat{\mathbf{p}}_i$  can be done independently), but keep the proper three-body phase space of the Dalitz plot [12,13].

Before this can be done, another complication has to be taken care of. The integrand  $\langle |(H')_{\text{fi}}|^2 \rangle_{\text{spin}}$  contains the propagator factor  $D^{-2}$  which depends on the external hadron energies  $E_i$  and certain internal baryon energies. The external hadron energies are angle-independent, but some of the internal baryon energies do depend on the integration angles. If such angle-dependent internal energies are replaced by suitable angle-averaged values, for example by the replacement

$$|\mathbf{p} - \mathbf{p}_3| \rightarrow \sqrt{\langle \mathbf{p}^2 \rangle + \mathbf{p}_3^2}, \quad (11)$$

the factor  $D^{-2}$  simplifies to an angle-independent approximant  $\langle D^{-2} \rangle$  that can be taken out of the angle integrations.

The remaining factor in the integrand is now

$$\langle |(H_2 H_3)_{\text{fi}}|^2 \rangle_{\text{spin}} = \prod_{i=2}^3 \langle |(H_i)_{\text{fi}}|^2 \rangle_{\text{spin}}, \quad (12)$$

where the state labels  $i, f$  in  $(H_i)_{fi}$  are the initial- and final-state labels appropriate for the interaction  $H_i$ . The two sets of angle integrations can now be done independently, leading to the “off-shell” two-body decay widths

$$\Gamma_i(W_i) = \frac{4\pi p_i^2 dp_i}{(2\pi)^2 dW_i} \langle |(H_i)_{\text{fi}}|^2 \rangle_{\text{spin,angle}}, \quad (13)$$

where

$$\langle |(H_i)_{\text{fi}}|^2 \rangle_{\text{spin,angle}} = \frac{1}{4\pi} \int \langle |(H_i)_{\text{fi}}|^2 \rangle_{\text{spin}} d^2\hat{\mathbf{p}}_i. \quad (14)$$

These decay widths are in general off-shell because the energy in each final state differs in general from that in the initial state. The effective energy  $W_i$  in the density of states remains to be chosen.

Eq. (7) has thus been simplified to

$$\Gamma \approx \frac{1}{2\pi} \int dW_2 dW_3 \left( \frac{E_1}{2p_2 p_3} \right) \Gamma_2(W_2) \langle D^{-2} \rangle \Gamma_3(W_3). \quad (15)$$

This is the basic angle-average approximation used in this paper. In this expression, the effective energies  $W_i$  are arbitrary integration variables to be chosen for convenience since the integral is actually independent of their choices. Whatever the choice, the remaining integrations should be performed over an appropriate Dalitz area that reproduces what is left of the three-body phase space after the angle integrations.

We choose  $W_3 = E_3$  so that  $\Gamma_3$  is actually the static limit [where  $m_\pi \ll m(\text{nucleon})$ ] of the physical width

for pion emission. We use  $W_2 = 2E_2$  in order to make the width  $\Gamma_2$  for Fig. 1a an off-shell  $d^* \rightarrow NN$  decay width with a two-body density of states defined for the  $N^2$  system of total energy  $2E_2$ .

The actual  $\pi NN$  decay amplitude is of course a sum over contributions from several Feynman diagrams, though limited in this section for convenience in presentation to only Figs. 1a-c. To treat their interference, we shall need the complex transition amplitudes for the  $BB$  recoil

$$F_i = \Gamma_i^{1/2} e^{i\phi_i} . \quad (16)$$

The final decay width will then be the sum of contributions

$$\Gamma = \sum_{\alpha, \beta} \Gamma(\alpha, \beta), \quad \text{with } \alpha, \beta = a, b, \text{ or } c, \quad (17)$$

where

$$\Gamma(\alpha, \beta) \approx \frac{4}{2\pi} \int dE_2 dE_3 \left( \frac{E_1}{p_2 p_3} \right) \times F_{2\alpha}^* F_{2\beta} \langle (D_\alpha D_\beta)^{-1} \rangle F_{3\alpha}^* F_{3\beta}, \quad (18)$$

if there were no additional complications in the angle and spin averages for the ‘‘off-diagonal’’ terms. An extra factor of 4 appears because there are two  $\Delta$ ’s in  $d^*$ . The diagonal terms  $\Gamma(\alpha, \alpha)$  are positive, while the interference terms  $\Gamma(\alpha, \beta \neq \alpha)$  could be negative.

Further development of this formula is possible under special circumstances. Matrix elements at corresponding vertices in different diagrams can be related to one another through the quark model [1,14]. For example, the  $\pi qq$  vertex for pion emission from quark  $i$  can be taken to be the NR expression

$$V_{\pi qq} = \frac{f_{\pi qq}}{m_\pi} (\boldsymbol{\sigma}_i \cdot \mathbf{p}_3) (\boldsymbol{\tau}_i \cdot \boldsymbol{\Phi}), \quad (19)$$

where  $\boldsymbol{\Phi}$  is the pion wave function, and  $f_{\pi qq} = (3/5)f_{\pi NN}$  is the coupling constant. The NR quark model can then be used to relate the  $B \rightarrow \pi N$  decay widths that appear in these Born diagrams to just the basic width

$$\Gamma_{3b}(p_3) = \Gamma(\Delta \rightarrow N\pi), \quad (20)$$

together with additional factors that represent changes in the reduced matrix elements of operators appearing in the interaction. Additional details will be given in the Appendix. Re-scattering effects for the emitted pion will not be included in the present study.

The  $BB \rightarrow NN$  transition is more complicated. The transition matrix element  $(H_2)_{fi}$  in Figs. 1b and c should be calculated in the  $d^*$  rest frame, not in the final-state  $N^2$  c.m. frame where the dynamics is usually specified. This means that

$$F_{2i}(W_2) = \delta_\rho \mathcal{F}_{2i}(p_2^*), \quad (21)$$

where

$$\delta_\rho = \sqrt{\frac{\rho_2}{\rho_2^*}} = \sqrt{\frac{p_2 E_2}{p_2^* E_2^*}}, \quad (22)$$

and  $\mathcal{F}$  is an off-shell transition amplitude containing the two-body density of states calculated in the  $N^2$  c.m. frame where the nucleon momentum is

$$p_2^* = \sqrt{\frac{1}{4}m_{12}^2 - m^2}, \quad (23)$$

and

$$m_{12} = (E_1 + E_2)^2 - p_3^2 \quad (24)$$

is the invariant mass of the  $N^2$  system.

We could still use the NR quark model to relate the different operator matrix elements of different diagrams so that the same basic transition amplitude  $\mathcal{F}_{2a}$  appears in different diagrams, albeit evaluated at different energies and with different additional factors. Finally, spin averages must be performed term by term for Eq. (17), as discussed in the Appendix. In this way, we get the final result for Figs. 1a-c of

$$\Gamma_{ac} \approx \frac{25}{12\pi} \int dE_2 dE_3 \left( \frac{E_1}{p_2 p_3} \right) \Gamma_{3b} \times \left| \frac{\mathcal{F}_{2a}(p_2)}{D_a} + \delta_\rho \left( \frac{2\mathcal{F}_{2a}(p_2^*)}{3D_b} + \frac{\mathcal{F}_{2a}(p_2^*)}{3D_c} \right) \right|^2, \quad (25)$$

involving angle-averaged quantities. This is the decay-width expression actually used in our calculations.

We could have used empirical  $mBB$  coupling constants [7] or some other model of  $mBB$  dynamics [14] instead of the NR quark model to calculate different  $BB$  recoil amplitudes. The result will differ somewhat from those shown in the equation. However, the differences are not expected to be very large from the viewpoint of the rough estimates attempted here. So we shall not consider these alternatives in this paper.

Equation (25) has a particularly simple structure if the recoil amplitude  $\mathcal{F}_{2a}$  is calculated in the Born approximation or evaluated at a common nucleon momentum  $p_2$  instead of at two different values. On ignoring the small difference in the density of states in different  $N^2$  frames as well, we find

$$\Gamma \approx \frac{25}{12\pi} \int dE_2 dE_3 \left( \frac{E_1}{p_2 p_3} \right) \Gamma_{3b} \Gamma_{2a} \times \left| \frac{1}{D_a} + \frac{2}{3D_b} + \frac{1}{3D_c} \right|^2, \quad (26)$$

where

$$\Gamma_{2a} = \Gamma(d^* \rightarrow N^2(^1D_2)). \quad (27)$$

This very rough formula for  $\Gamma$  shows that the relative importance of the diagrams is approximately controlled by the energy denominators  $D_i$ .

To estimate these energy denominators, we note that an external nucleon has the median energy of

$$E(\mathbf{p}_2) \approx \frac{1}{2}(m_N + E_{\max}) = 961 \text{ (988) MeV}, \quad (28)$$

where the numerical value is for  $m^* = 2100 \text{ (2200) MeV}$ . For small  $d^*$  masses, the internal baryon energies that appear are dominated by the internal momentum  $\mathbf{p}$  of  $d^*$  of radius  $r^*$  (usually taken to be 0.7 fm):

$$\langle \mathbf{p}^2 \rangle = \frac{9}{16r^{*2}} \approx (210 \text{ MeV}/c)^2, \quad (29)$$

$$E(\mathbf{p}) \approx \sqrt{m_N^2 + \langle \mathbf{p}^2 \rangle} = 962 \text{ MeV}, \quad (30)$$

$$E_\Delta(\mathbf{p}) \approx \sqrt{m_\Delta^2 + \langle \mathbf{p}^2 \rangle} = 1250 \text{ MeV}, \quad (31)$$

and  $E_i(\mathbf{p} - \mathbf{p}_3) \approx E_i(\mathbf{p})$ . These gives the rough estimates at  $m^* = 2100 \text{ (2200) MeV}$  of

$$\begin{aligned} D_a &\approx 178 \text{ (224) MeV}; \\ D_b &\approx -290 \text{ (-236) MeV}, D_c \approx -578 \text{ (-524) MeV}. \end{aligned} \quad (32)$$

These approximate energy denominators can be used in Eq. (26) to show that the decay widths from the three diagrams taken individually are roughly in the ratio

$$\Gamma(a, a) : \Gamma(b, b) : \Gamma(c, c) \approx 1 : (-0.41)^2 : (-0.10)^2 \quad (33)$$

at 2100 MeV, and

$$\Gamma(a, a) : \Gamma(b, b) : \Gamma(c, c) \approx 1 : (-0.63)^2 : (-0.14)^2 \quad (34)$$

at 2200 MeV. Because the denominator of Fig. 1a has sign opposite to those in Figs. 1b and c, the amplitude from this dominant process interferes destructively with those from the latter diagrams, as shown explicitly in the last two equations. This destructive interference leads to a total decay width for Figs. 1a-c that is roughly an order of magnitude smaller than  $\Gamma_a$  from Fig. 1a alone.

#### IV. RESULTS FOR $D^* \rightarrow \pi NN$

To obtain a  $\pi NN$  decay width  $\Gamma$ , we need to integrate Eq. (25) over the three-body phase space left over after angle integrations. It seems useful to give a rough order-of-magnitude estimate of the dominant term  $\Gamma_a$  from Fig. 1a as we go over some of the technical details involved in the integration.

The two-body width for P-wave pion emission is best expressed in terms of the experimental decay width  $\Gamma_\Delta \equiv$

$\Gamma(\Delta \rightarrow \pi N)$  of 120 MeV for a free  $\Delta$  of mass  $m_\Delta = 1232$  MeV:

$$\Gamma_{3b} = \Gamma_\Delta \left( \frac{p_3 m_\Delta}{k^* E_N^*} \right) \left( \frac{p_3}{k^*} \right)^2 e^{\alpha(k^{*2} - p_3^2)}, \quad (35)$$

where the starred parameters are in the  $\Delta$  c.m. frame:

$$k^* = 227 \text{ MeV}, \quad E_N^* = 966 \text{ MeV}. \quad (36)$$

The Gaussian factor comes from a baryon formfactor calculated by using Gaussian wave functions in a NR quark model. It depends on a parameter

$$\alpha = r_p^2/6 = 1.54 \times 10^{-6} \text{ MeV}^{-2}. \quad (37)$$

related to the proton radius  $r_p$ . The value of  $r_p = 0.6$  fm used here is the one commonly used in many NR quark models, including [2]. It is not the experimental proton charge radius. Note that the pion momentum  $p_3$  appearing in Eq.(35) is that in the  $d^*$  rest frame, and that the distortion of the outgoing pion wave function has been neglected.

Momentarily ignoring the Gaussian factor from the baryon formfactor, we find for  $m^* = 2100 \text{ (2200) MeV}$

$$\begin{aligned} \Gamma_{3b \max} &= 59 \text{ (256) MeV}, \\ \left\langle \frac{\Gamma_{3b}}{p_3} \right\rangle &\approx \frac{\Gamma_{3b \max}}{2.5 p_{3 \max}} = 0.14 \text{ (0.38)}; \end{aligned} \quad (38)$$

at the maximum value  $p_{3 \max} = 165 \text{ (270) MeV}$  of  $p_3$ . The average shown in the last expression involving a denominator factor of 2.5 is obtained as follows: For non-relativistic (extremely relativistic) kinematics, the phase space is roughly rectangular in  $p_3^2$  ( $p_3$ ). The average then has a denominator factor of 2 (3). For most of the pion energies studied here, the kinematics is neither nonrelativistic and extremely relativistic. So we take a denominator factor of 2.5.

The two-body width  $\Gamma_{2a}(p_2)$  for the two-body decay  $d^* \rightarrow NN$  is much less familiar, but it has recently been studied in [1]. It is given by Eq. (38) of that paper, an expression that works for any final nucleon momentum  $p_2$  in the rest frame of the final-state  $N^2$  system. It can be used for the off-shell momenta appearing in our diagrams, provided that the reduced mass  $\mu_f^*$  appearing in the equation is taken to be  $E_2/2$  (where  $E_2 = \sqrt{p_2^2 + m^2}$ ) and not  $m^*/4$ .

Different dynamical inputs are possible. We use the full Bonn (FB) potential in the Born approximation, a choice referred to below as the FB model. Of course, the Born approximation of a static potential is rather crude because it contains no off-shell effect, but it represents a familiar starting point. The resulting width parameter  $\Gamma_{2a}(p)/p^2$  is shown by a solid curve in Fig. 3 as a function of the nucleon momentum  $p$  in the c.m. frame of the final  $NN$  state.

Certain re-scattering effects not included in Fig. 1 could be included by using empirical  $NN$   $t$ -matrices constructed by Love and Franey (LF) [6] from experimental  $NN$  phase shifts. These empirical  $t$ -matrices are of course on-shell  $NN$   $t$ -matrices, but here evaluated at the same momentum transfer  $q$  as the needed off-shell  $t$ -matrices. So no dynamical off-shell effects can be included here. To my best knowledge, there is no simple way to extrapolate these empirical  $t$ -matrices off-shell without using a realistic potential model.

These LF on-shell  $t$ -matrices are actually energy dependent. In Fig. 1a, the  $t$ -matrix involved is that for the initial dibaryon state of mass  $m^*$ . We therefore use the empirical  $t$ -matrix at the  $N^2$  energy of  $\sqrt{s} = m^*$ .

Now the  $d^* \rightarrow NN$  decay in free space gives two nucleons each of momentum  $p_{\max}$ . The resulting decay width is represented by a solid circle in Fig. 3. In Fig. 1a, on the other hand, we need decay widths at the same  $\sqrt{s} = m^*$  but with off-shell nucleon momentum  $p < p_{\max}$ . They can also be calculated for the same  $t$ -matrix input from the decay width formula of [1] because this formula works for any nucleon momentum. The result is shown as a dashed curve in Fig. 3, one for each  $\sqrt{s}$  whose value (in MeV) is also given near the curve. These  $t$ -matrices are said to be calculated at the (initial-state) dibaryon energy (or DBE).

In contrast, the recoil interaction in Figs. 1b or 1c takes place after pion emission, i.e. at lower energies. It involves an off-shell  $t$ -matrix defined at the energy of the final  $N^2$  state, as in the analogous processes in  $pp$  bremsstrahlung [15–17]. In the present rough estimate, it is convenient to interpret it as an off-shell  $BB \rightarrow NN$  decay process at an intermediate  $B^2$ -state energy  $\sqrt{s} < m^*$ . This means that one should use points from the dashed curves in Fig. 3 at smaller c.m. energies. The figure shows that such decay widths are smaller because the empirical  $t$ -matrix is found to decrease rapidly as  $\sqrt{s}$  decreases.

Such a strong energy dependence originates from the strong energy dependence of certain empirical  $NN$  phase parameters such as the mixing parameter  $\epsilon_1$  in the  $N^2(^3S_1 - ^3D_1)$  states. The LF  $t$ -matrices we use were constructed in [6] from the energy-dependent phase solution SP84 of Arndt and collaborators [18]. It is well-known that the energy-dependent mixing parameter  $\epsilon_1$  from SP84 already varies more smoothly and more slowly with energy than the so-called single-energy solutions. Nevertheless, it still has an energy dependence much stronger than that of any common  $NN$  potential such as the FB potential. This situation can be seen in Fig. 15-7 of [5]. In other words, the empirical  $t$ -matrices and the FB potential do not represent exactly the same dynamical input when it comes to this tricky isovector tensor-force part of the  $NN$  interaction.

Given this complication, and the other problem of missing off-shell dynamics, we decide to use a much

cruder approach for these empirical  $t$ -matrices. Instead of using them at different effective  $B^2$  energies dictated by each diagram, we shall use two extreme prescriptions meant to provide rough upper and lower bounds.

The first prescription is to use  $t$ -matrices of the same  $NN$  energy  $\sqrt{s} = m^*$  in all decay diagrams, i.e. using only points lying on one of the dashed curves in Fig. 3. These  $t$ -matrices are thus calculated at the initial-state dibaryon energy, a prescription referred to below as the LF-DBE model. One can see from Fig. 3 that the resulting decay widths are larger than those calculated at variable energies. The DBE results for  $\Gamma_{\pi NN}$  can therefore be expected to be rough upper bounds. Fig. 3 shows that these DBE results are likely to be close to those calculated with the FB dynamics.

The second prescription uses  $t$ -matrices calculated at the lowest possible energies in order to generate a rough lower bound. These energies will be taken to be  $NN$  energies (NNE) after the recoil, giving a prescription to be called the LF-NNE model. The resulting  $\Gamma_{2a}$  decay widths are the free-space widths reported in [1] and represented by solid circles in Fig. 3. In other words, the solid circles are now treated as a function of the nucleon momentum  $p_2$  and used in all diagrams. We can see from Fig. 3 that the  $\Gamma_{\pi NN}$  that results will be much smaller than those for the LF-DBE or FB models. Since the LF-DBE model does not contain the effects of decreased effective  $B^2$  energies for the recoil after pion emission while the LF-NNE model uses  $NN$  energies that are far too low, the actual LF results can be expected to be somewhere between these two LF models.

Although we have not calculated the full off-shell  $t$ -matrix from the FB potential, it is nevertheless useful to point out some expected re-scattering effects in it. We shall concentrate on  $\Gamma_{2a}$ , where the  $\Delta^2(^7S_3) \rightarrow N^2(^3D_3)$  matrix element of the isovector tensor force has the same sign as the  $N^2(^3S_1) \rightarrow N^2(^3D_1)$  matrix element, according to Eqs. (A3) and (A4). The long-range part of this isovector tensor force is from pion exchange and is attractive in the  $N^2(^3S_1 - ^3D_1)$  states. Hence re-scatterings can be expected to enhance its contribution, i.e. to increase the width in Fig. 3 for small momenta. On the other hand, the short-range part of the tensor force is dominated by rho exchange, and is repulsive. Re-scatterings will then reduce its value, leading to a decreased width in Fig. 3 at large momenta. These considerations suggest that with re-scatterings, the width from the FB model is likely to move towards that for the LF-DBE model. Even though we do not know the quantitative extent of the change, we do expect the actual results to be much closer to the LF-DBE or FB values than the LF-NNE values. This is especially true if the mixing parameter  $\epsilon_1$  given by the FB potential is more realistic than the empirical values obtained from phase-shift analysis.

To summarize, the three models shown in Fig. 3 seem to present an interesting range of dynamics for our rough

estimate of the  $\pi NN$  decay width.

Let us now return to our rough estimate of  $\Gamma_a$  using the FB model for  $\Gamma_{2a}$ . We average the dimensionless “reduced” width  $\Gamma_{2a}/p_2$  by itself over a rectangular distribution of  $p_2^2$  (for approximately nonrelativistic kinematics) to get the rough estimate

$$\begin{aligned} \left\langle \frac{\Gamma_{2a}}{p_2} \right\rangle &\approx \frac{1}{p_{2\max}^2} \int_0^{p_{2\max}^2} \frac{\Gamma_{2a}(p)}{p} d(p^2) \\ &= 0.010 \text{ (0.022)} \end{aligned} \quad (39)$$

for  $m^* = 2100$  (2200) MeV.

The energy denominator  $D_a$  is next factored out of the integral by using the median energy  $\langle E_1 \rangle$  of  $E_1$  given in Eq. (28). After replacing the factor  $E_1$  in the integrand itself by its median value, we are finally left with an integration over the  $E_2 E_3$  (or  $N\pi$ ) Dalitz area [13]

$$A = \int_{\text{Dalitz}} dE_2 dE_3. \quad (40)$$

This area turns out to be 1390 (6800) MeV<sup>2</sup>. Hence

$$\begin{aligned} \Gamma_a &\approx \frac{25}{12\pi} A \left\langle \frac{\Gamma_{2a}}{p_2} \right\rangle \frac{\langle E_1 \rangle}{\langle D_a \rangle^2} \left\langle \frac{\Gamma_{3b}}{p_3} \right\rangle \\ &\approx 0.04 \text{ (0.7) MeV}, \end{aligned} \quad (41)$$

for the FB potential. As expected, the three-body decay width increases sharply with increasing  $m^*$ . It is also rather small, even before the destructive interference with the other amplitudes is included.

It is now a simple matter to return to Eq. (25) and perform an honest integration over the Dalitz area without making the separate averages described previously in this section. In the energy denominators, we use the actual external energies  $E(\mathbf{p}_1)$  and  $E(\mathbf{p}_2)$  of each point in phase space, the approximate internal energies for  $E_i(\mathbf{p})$  shown in Eqs. (30) and (31), and the approximation

$$E_i(\mathbf{p} - \mathbf{p}_3) \approx \sqrt{m_i^2 + \langle \mathbf{p}^2 \rangle} + p_3^2, \quad (42)$$

that is the leading term of a Legendre expansion in  $\mathbf{p} \cdot \mathbf{p}_3$ . The calculated results from Fig. 1a alone are shown in Fig. 4 as a light solid curve for the FB model, as open diamonds for the LF-DBE model, and as a light dashed curve the LF-NNE model. The results for Figs. 1a-c are shown as a heavy dotted curve for the FB model, solid squares for the LF-DBE model, and a dot-dashed curve for the LF-NNE model.

We see that the results from all three models are in better agreement the higher the  $d^*$  mass. The FB and LF-DBE results are quite close to each other over the entire mass range, with the LF-DBE widths a little larger close to the threshold, and a little smaller as  $m^*$  increases beyond 2100 MeV. The LF-NNE widths are about an order of magnitude smaller than those from the other two

models below 2100 MeV. Hence the FB widths seem to be quite reasonable, being comfortably within our rough upper and lower bounds at low  $d^*$  masses.

Figure 4 also shows clearly how the destructive interference among Figs. 1a-c reduces their resultant decay width significantly, as we have already noted previously.

## V. RETARDATION AND PAIR CONTRIBUTIONS

The remaining six diagrams shown in Fig. 1 come in two groups: Figs. 1d-f describe the retardation contributions due to pion emissions from a baryon when a virtual meson is in the air, while Fig. 1g-i describe pion emission via the creation of a  $B\bar{B}$  pair.

The propagator for the retardation diagram  $\alpha$  contains the energy-denominator factors  $D_0^{-1} D_\alpha^{-1}$ , where the initial-state energy denominator

$$D_0 = m^* - \omega - E(\mathbf{p}_2) - E_\Delta(\mathbf{p}) \quad (43)$$

is the same in all three diagrams. Note that the sum of the two intermediate-state baryon energies that appears is only about 2210 (2240) MeV for  $m^* = 2100$  (2200) MeV. That is, this energy sum increases very slowly beyond the sum of their rest energies (at 2170 MeV) as  $m^*$  increases. Hence for  $m^* \approx 2200$  MeV,  $D_0$  is close to  $-\omega$ , where  $\omega = \sqrt{m_m^2 + q^2}$  is the meson energy.

The final-state energy denominator  $D_\alpha$  depends somewhat on the diagram  $\alpha$  with:

$$\begin{aligned} D_d &= E(\mathbf{p}_2) - \omega - E_\Delta(\mathbf{p}), \\ D_e &= E(\mathbf{p}_1) - \omega - E(-\mathbf{p} - \mathbf{p}_3), \\ D_f &= E(\mathbf{p}_1) - \omega - E_\Delta(-\mathbf{p} - \mathbf{p}_3). \end{aligned} \quad (44)$$

All angle-dependent energies will eventually be approximated by angle-averaged energies.

We turn next to the integration over one of the internal momenta, say the meson momentum  $\mathbf{q}$ . (The other internal momentum  $\mathbf{p}$  is then fixed by momentum conservation.) This integration works out the same way it does for the two-body transition amplitude  $\mathcal{F}$  of Fig. 1a-c [1]. The major difference is that the meson propagator  $\omega^{-2}$  for Figs. 1a-c is now replaced by the propagator  $1/\omega D_0 D_\alpha$  for a retardation diagram  $\alpha$ . The appearance of an additional  $\omega$ -dependent energy denominator has the consequence that the longer-range  $\pi$ -exchange contribution becomes relatively more important than in Figs. 1a-c.

This change of propagator causes some complication in the calculation. Since the additional energy denominator depends on the meson mass, it can be included only if the  $\pi$ - and  $\rho$ -exchange contributions can be separated. The transition amplitude  $\mathcal{F}$  from Figs. 1a-c is of course separable into the form:



$$\mathcal{F} = \mathcal{F}_\pi + \mathcal{F}_\rho \quad (45)$$

when the virtual-meson exchange is treated literally in the Born approximation implied by the figures. By the same argument, the retardation diagrams 1d-f taken literally as Born diagrams give rise to transition amplitudes  $\mathcal{R}$  of the same separable form

$$\mathcal{R} = \mathcal{R}_\pi + \mathcal{R}_\rho. \quad (46)$$

The situation is more complicated when re-scattering effects are also included, for example, by using the LF  $t$ -matrices. While the amplitude  $\mathcal{F}$  can be calculated without the separation of terms shown in Eq. (45), the calculation of  $\mathcal{R}$  is not possible without it. Fortunately, each LF  $t$ -matrix is made up of a sum of three or four terms with different effective meson masses, although the function used differs somewhat from that appearing in one-boson exchange potentials. Hence the calculation of  $\mathcal{R}$  is still possible if one interprets these terms as the separate contributions from different mesons or groups of mesons.

This prescription is admittedly far from ideal, but even a theoretically calculated  $t$ -matrix may not be separable into terms describing single-meson exchanges. The reason is simply that re-scattering means the inclusion of terms with two or more exchanged mesons. Their correct treatment can only be based on Feynman diagrams. In spite of this limitation, a calculation using the empirical  $t$ -matrix should still be very informative. The actual formula used to calculate  $\mathcal{R}$  for LF  $t$ -matrices will be given in the Appendix.

One final problem in using the LF  $t$ -matrices has to be mentioned. The longest-range part of their tensor  $t$ -matrices is not one with the pion mass, but one with twice the mass. The authors found the constraint to match the one-pion range “too restrictive” [6], though they were successful in constraining the longest-range term of the real part of the central  $t$ -matrices to the one-pion value. This range problem is probably not serious in generating the amplitude  $\mathcal{F}$ , but possibly more serious in the amplitudes  $\mathcal{R}$  for retardation diagrams. This is because these diagrams contain one more energy denominator dependent on the meson energy  $\omega$ . If the meson mass is too large in these energy denominators, the resulting decay amplitudes might be too small. It is hard to tell if this is indeed the case for a numerically fitted function as there might be compensating terms in the fit, but we shall watch out for this possibility in the calculated results.

We turn next to the pair diagrams of Figs. 1g-i. Since we need a rank-3 spin operator for the decay  $d^*[\Delta^2(^7S_3)] \rightarrow \pi NN$ , the pion-emission vertex has to be spin-dependent, while the virtual-meson exchange from or to the pair must involve a rank-2 spin operator. The spin-dependent part of the pion emission vertex with the creation or annihilation of a  $B\bar{B}$  pair turns out to be of order  $p/m$  (ratio of baryon momentum to baryon mass)

relative to the spin-dependent pion emission vertex from a baryon. The rank-2 spin part of the  $B^2\bar{B} \rightarrow B$  interaction turns out to be also of order  $p/m$  relative to the rank-2 spin operator in the nonrelativistic  $BB \rightarrow BB$  interaction for both  $\pi$  and  $\rho$  exchanges. Furthermore, the additional energy denominator for these pair diagrams is larger in absolute value than those in Figs. 1a-f by roughly twice the baryon mass. The consequence is that these pair contributions to the decay amplitude can be expected to be roughly two orders of magnitude smaller than those for the other diagrams of Fig. 1 in the mass region of interest in this paper. They can therefore be neglected.

Returning now to the retardation amplitudes  $\mathcal{R}$ , we need to add them to Eq. (25) and perform spin averages in the same way as for Figs. 1a-c. Again, it will be convenient to express all operator matrix elements for the retardation diagrams in terms of that appearing in Fig. 1d for which the transition amplitude is  $\mathcal{R}_{2d}$ , where the subscript 2 refers to the “spectator” nucleon. The final expression for the  $\pi NN$  width for Figs. 1a-f turns out to have the same structure as Eq. (25):

$$\Gamma_{af} \approx \frac{25}{12\pi} \int dE_2 dE_3 \left( \frac{E_1}{p_2 p_3} \right) \Gamma_{3b} \times \left| \mathcal{B}(a, d) + \delta_\rho \left( \frac{2}{3} \mathcal{B}(b, e) + \frac{1}{3} \mathcal{B}(c, f) \right) \right|^2, \quad (47)$$

where

$$\begin{aligned} \mathcal{B}(a, d) &\approx \mathcal{R}_{2d}(d; p_2) + \frac{\mathcal{F}_{2a}(p_2)}{D_a}, \\ \mathcal{B}(b, e) &\approx \mathcal{R}_{2d}(e; p_2^*) + \frac{\mathcal{F}_{2a}(p_2^*)}{D_b}, \\ \mathcal{B}(c, f) &\approx \mathcal{R}_{2d}(f; p_2^*) + \frac{\mathcal{F}_{2a}(p_2^*)}{D_c} \end{aligned} \quad (48)$$

are amplitudes for pion emission from a baryon. The diagram labels  $a - f$  are kept in the expressions as they define the energy denominators to be used in the amplitudes.

To simplify the calculation of the retardation amplitudes, we use in the energy denominators  $D_e$  and  $D_f$  the approximation

$$\begin{aligned} E_i(-\mathbf{p} - \mathbf{p}_3) - E(-\mathbf{p}_2 - \mathbf{p}_3) &\approx \\ E_i(-\mathbf{p}) - E(-\mathbf{p}_2), \end{aligned} \quad (49)$$

where  $i = \Delta$  or  $N$  (i.e., blank). The mean external nucleon energy defined in Eq. (28) is used for  $E(\pm\mathbf{p}_2)$ , and the r.m.s. momentum  $\langle \mathbf{p}^2 \rangle^{1/2}$  of the initial state is used in the internal energies  $E_i(\mathbf{p})$ .

The resulting  $\pi NN$  decay width  $\Gamma_{af}$  is shown as a solid curve for the FB model, and as solid circles for the LF-DBE model. For comparison, the partial width  $\Gamma_a$  for Fig. 1a alone is also shown, as a light solid curve for the

FB model, and open diamonds for the LF-DBE model. All these widths have been calculated for a  $d^*$  radius of 0.7 fm. The width  $\Gamma_{af}$  for a  $d^*$  radius of  $r^* = 0.9$  (0.5) fm is also shown in the figure as a long-dashed (dashed) curve.

The main feature seen in Fig. 5 is that the retardation diagrams have overcome the reduction caused by the destructive interference among Figs. 1a-c to give a more normal result quite close to  $\Gamma_a$  for Fig. 1a alone. It is interesting that  $\Gamma_{af}$  is greater than  $\Gamma_a$  for the FB model, but smaller for the LF-DBE model. The difference has a simple explanation.

First of all, we should recall that the decay at the  $BB \rightarrow NN$  step is controlled by a competition between the long-range attractive tensor force from  $\pi$ -exchange and the shorter-range repulsive tensor force from  $\rho$ -exchange [1]. This cancellation makes the width increase less rapidly with increasing dibaryon mass. It also explains why the width is smaller for a dibaryon of smaller size, as seen in Fig. 5.

Now the retardation diagrams contain an extra energy denominator that depends on the meson mass, a feature that favors the contribution from the virtual meson of smaller mass. Consequently, the attractive  $\pi$ -exchange contribution is re-inforced in the FB model. In the LF models, the one-pion term is absent in the isovector tensor force. The terms that remain correspond to larger meson masses giving larger energy denominator, and hence smaller retardation contributions.

If this picture is correct, the FB result would appear to be more sensible. However, a careful study of both theoretical  $t$ -matrices calculated from potential models and empirical  $t$ -matrices constructed from phase shifts will be needed to confirm this interpretation. We have not calculated the results for the TF-NNE model, but they are likely to be much smaller.

Our general conclusion is that while the energy dependence of the  $t$ -matrix is not insignificant, the best estimate we have now is based on the FB model. According to Fig. 5, it gives a value of  $\Gamma_{af}$  for Figs. 1a-f that is about 0.006 (0.07, 0.5) MeV at  $m^* = 2065$  (2100, 2150) MeV.

## VI. $\ell$ FORBIDDENNESS AND THRESHOLD BEHAVIORS

It is now useful to discuss the threshold behavior of the decay width. We shall begin with the Dalitz area  $A(m^*)$  defined in Eq. (40). In the NR limit, it varies with momenta roughly as  $(p_{2\max}p_{3\max})^2$ . In reality, the dependence is only a little weaker than this, as the dotted curve for the ratio

$$C_A(m^*) = A(m^*)/(p_{2\max}p_{3\max})^2 \quad (50)$$

of  $A$  to its threshold behavior shows in Fig. 6.

Using the NR dependence for the Dalitz area, we find a threshold behavior for the 3-body decay of

$$\Gamma(m^*) \approx \text{const } p_{3\max}^{2\ell_\pi+2} p_{2\max}^{2\ell_N+2}. \quad (51)$$

This dependence could be approximated by just  $p_{2\max}^{2\ell+4}$ , where  $\ell = \ell_\pi + \ell_N$  is the degree of forbiddenness of the decay, but we shall not make this additional approximation here.

For  $d^* \rightarrow \pi NN$  with P-wave pion emission, we have  $\ell_\pi = 1$ ,  $\ell_N = 2$ , and a decay that is third forbidden. To see how dominant this threshold power law is, we show in Fig. 6 the ratios

$$C_\alpha(m^*) = \Gamma_\alpha(m^*)/(p_{3\max}^4 p_{2\max}^6), \quad (52)$$

where  $\alpha = a$  and  $af$ , as functions of the  $d^*$  mass for both the partial width  $\Gamma_a$  from Fig. 1a only (dashed curve) and the width  $\Gamma_{af}$  from Figs. 1a-f (solid curve). Both widths are calculated with the FB model of interactions.

These curves show that the threshold behavior is further modified by momentum dependences due to dynamics and form factors. In fact, both decay widths behave roughly as  $p_{3\max}^4 p_{2\max}^5$  over the first half of the mass range shown in the figure, a small reduction in the momentum power being used to simulate the significant momentum dependences shown in the figure.

These results are relatively simple because the initial state is a relative S-state. The situation is more complicated for a relative D-state. The solid spherical harmonic  $\mathcal{Y}_{2m}(\mathbf{p})$  that appears in the initial-state wave function would have given rise to an additional factor of

$$p^2 = (\mathbf{p}_2 + \mathbf{q})^2, \quad (53)$$

where  $\mathbf{q}$  is the momentum of the virtual meson involved in the  $BB$  recoil. Since this internal momentum is eventually integrated over, what survives of the  $q^2$  term has the same threshold behavior as those from the S-state component of  $d^*$ . The remaining terms in the equation have additional powers of the external momentum  $p_2$  left over, leading to amplitudes with higher powers of  $p_2$ .

We have shown in Sec. II that the  $d^*$  decay by S-wave pion emission is also third forbidden. This S-wave emission comes from the second, or S-wave, term in the basic  $\pi qq$  vertex calculated from the usual  $\pi qq$  Lagrangian with either pseudovector or pseudoscalar coupling:

$$V_{\pi qq} = \text{const}[-\boldsymbol{\sigma} \cdot (\mathbf{p} - \mathbf{p}') + (w/4m)\boldsymbol{\sigma} \cdot (\mathbf{p}' + \mathbf{p})] \quad (54)$$

in the NR and  $w \ll m$  limit [8]: Here  $\mathbf{p}$  ( $\mathbf{p}'$ ) is the quark momentum before (after) pion emission, the momentum of the emitted pion being  $\mathbf{p}_3 = \mathbf{p} - \mathbf{p}'$ , and  $w = E - E'$  is the baryon energy transfer. One can show that for  $d^*$  decay, the use of the second term, the S-wave  $\pi qq$  vertex, instead of the first, or P-wave, vertex results in the substitution of one power of the pion momentum  $p_3$

by one power of the  $NN$  relative momentum  $|\mathbf{p}_1 - \mathbf{p}_2|$  in the final state. This substitution leaves the threshold power law unchanged.

However, it is not true that the threshold power law is always determined completely by the degree of forbiddenness of the decay. Occasionally the expected threshold term is absent. Then the surviving leading terms are higher-order Taylor terms with a momentum power greater than expected. This situation will be described as being “unfavored” because an increase in the power implies a reduction in the decay width near threshold. So the general rule for the threshold power law is that the power is not smaller than that determined by the  $\ell$ -forbiddenness of the decay, but it could be bigger if the decay is unfavored.

To support the assertion that some decay amplitudes are unfavored, I now describe an example which is interesting in its own right. It is the  $\pi NN$  decay of that most promising of low-mass dibaryons, namely  $d'$  ( $J^\pi = 0^-, T = 0$  or  $2$ ), which was first proposed for a dibaryon interpretation of the structures seen in the pionic double charge exchange reaction  $nn(\pi^+, \pi^-)pp$  on nuclear neutrons [19–21].

The decay equations for S- and P-wave pion emissions are, respectively

$$d'(0^-, T = 0, 2) \rightarrow N^2(^1S_0) + \pi(\ell_\pi = 0). \quad (55)$$

$$d'(0^-, T = 0, 2) \rightarrow N^2(^3P_1) + \pi(\ell_\pi = 1); \quad (56)$$

This shows that S-wave pion emission is  $\ell = 0$  allowed, while P-wave pion emission is  $\ell = 2$  forbidden. This classification suggests that S-wave pion emission would normally dominate the decay near threshold.

A more detailed analysis shows that this is not always true. To see this, let us start with the simple models of  $d'$  used in [22]: a  $\Delta N$  bound state in a relative P-state for the  $T = 2$  dibaryon, and an  $N^*N$  relative-S bound state involving a P-state  $N^*$  for the  $T = 0$  dibaryon.

In the  $\Delta N$  model of  $d'(T = 2)$ , the off-shell  $\Delta$  can decay into a nucleon while the spectator nucleon can come out without further interaction. The pion emission vertex can be written in one of the following two forms when specialized to the three-body final state

$$V_{\pi N \Delta} = \text{const}[\boldsymbol{\sigma} \cdot \mathbf{p}_3 + (w/2m)\boldsymbol{\sigma} \cdot \mathbf{p}_{12}], \quad (57)$$

$$V_{\pi N \Delta} = \text{const} \left[ \left(1 - \frac{w}{4m}\right) \boldsymbol{\sigma} \cdot \mathbf{p}_3 - \frac{w}{2m} \boldsymbol{\sigma} \cdot \mathbf{p}_2 \right], \quad (58)$$

where

$$\mathbf{p}_3 = \mathbf{p}_\pi, \quad \mathbf{p}_{12} = \frac{1}{2}(\mathbf{p}_1 - \mathbf{p}_2) = -\mathbf{p}_2 - \frac{1}{2}\mathbf{p}_3 \quad (59)$$

in the dibaryon rest frame, and where  $\boldsymbol{\sigma}$  now stands for a transition spin operator [7]. We shall call these expressions the Jacobi form and the single-particle form, respectively.

The spectator nucleon (of momentum  $\mathbf{p}_2$ ) is a real spectator when final-state interactions are neglected. Its P-state wave function is

$$\psi_{1m}(\mathbf{p}_2) = f_1(p_2)\mathcal{Y}_{1m}(\mathbf{p}_2), \quad (60)$$

where the radial function  $f_1$  is finite at  $p_2 = 0$ .

Using the single-particle form for the pion emission vertex, we find that the first, or P-wave, vertex gives a decay amplitude proportional to  $\mathcal{Y}_{1m}(\mathbf{p}_2)\boldsymbol{\sigma} \cdot \mathbf{p}_3$ , while the S-wave vertex gives one proportional to  $\mathcal{Y}_{1m}(\mathbf{p}_2)\boldsymbol{\sigma} \cdot \mathbf{p}_2$ . One can recognize the presence of a P-wave pion in the first decay amplitude, and an S-wave pion in the second amplitude. However, both amplitudes depend on the external hadron momenta to the same second power.

It is easy to see why the naively-expected threshold term for S-wave pion emission is missing. The S-wave vertex is actually a three-body interaction that is P-wave in the spectator momentum  $\mathbf{p}_2$ . Multiplication into the initial P-state wave function gives an extra factor of  $p_2^2$ . In other words, the normal S-wave result at threshold, assumed to be momentum-independent, is simply absent. What survives is a higher-order term. We shall call attention to this abnormal situation by calling the decay unfavored.

An amusing complication in this decay of the  $\Delta N$  model  $d'(T = 2)$  is worth pointing out. In terms of the Jacobi momentum  $\mathbf{p}_{12}$  of the final  $N^2$  state, the initial P-state becomes a mixture of P- and S-states:

$$\begin{aligned} \mathcal{Y}_{1m}(\mathbf{p}_2) &= \mathcal{Y}_{1m}(-\mathbf{p}_{12} - \frac{1}{2}\mathbf{p}_3) \\ &= -\mathcal{Y}_{1m}(\mathbf{p}_{12}) - \frac{1}{2}\mathcal{Y}_{1m}(\mathbf{p}_3). \end{aligned} \quad (61)$$

This is caused by the recoil of the  $NN$  system on pion emission. The second term on the right-hand side describes the process where the pion carries away the orbital angular momentum leaving the  $N^2$  pair in a relative S-state.

The Jacobi description gives four amplitudes: Two are similar to those already described: a term proportional to  $\mathcal{Y}_{1m}(\mathbf{p}_{12})\boldsymbol{\sigma} \cdot \mathbf{p}_3$  for P-wave pion emission, and a term proportional to  $\mathcal{Y}_{1m}(\mathbf{p}_{12})\boldsymbol{\sigma} \cdot \mathbf{p}_{12}$  for S-wave pion emission. However, two additional terms appear:  $\mathcal{Y}_{1m}(\mathbf{p}_3)\boldsymbol{\sigma} \cdot \mathbf{p}_{12}$  describing P-wave emission from the S-wave vertex, and finally  $\mathcal{Y}_{1m}(\mathbf{p}_3)\boldsymbol{\sigma} \cdot \mathbf{p}_3$  describing S- and D-wave pion emissions from the P-wave vertex. These unexpected terms have their orbital angular momentum changed by baryon recoil on pion emission. The D-wave term comes with an  $NN(^1D_2)$  pair in the final state. It is  $\ell = 4$  forbidden, and is therefore quite unimportant. These recoil-induced emissions are present in the single-particle form as well, but one has to know where to find them.

One can see from Eq. (57) that the recoil-induced S-wave pion emission amplitude is not less important than the direct S-wave pion emission amplitude from the S-wave vertex, because unlike the latter it is not reduced

by the additional factor  $w/2m$ . However, it generates the same unfavored S-wave threshold behavior of a quadratic dependence on the external momenta and not the normal behavior independent of external momenta. So none of the S-wave decay amplitudes in our simple model of  $d'(T=2)$  is normal, and all are unfavored by two powers of the external momenta.

The above analysis is helpful because it tells us how to generate S-wave emission amplitudes that are normal and therefore dominant near threshold: The unwanted momentum can be prevented from appearing as an external momentum in an S-wave emission amplitude if it can be changed into an internal momentum that is eventually integrated over. This means that the P-wave excitation of the initial state should not be in the relative  $BB$  coordinate, but in a quark coordinate internal to a baryon. In other words, amplitudes with normal S-wave threshold behavior can only come from those components of  $d'(T=2)$  containing a P-wave excited  $\Delta^*$  or  $N^*$ .

The contributing term can readily be isolated by using a shell-model configuration in which a P-state quark in  $B^*$  becomes an S-state quark in a nucleon after pion emission. The angular integrations over the initial-state quark momentum  $\mathbf{p}$  has the form

$$\int d^2\hat{\mathbf{p}} \mathcal{Y}_{1m}(\mathbf{p}) V_{\pi qq} \exp[-b(\mathbf{p} - \mathbf{p}_3)^2], \quad (62)$$

where the solid spherical harmonic comes from the initial P-state and the Gaussian comes from the final S-state wave function. Using the single-particle form Eq. (58) of the  $\pi NN$  vertex with  $\mathbf{p}_2 = -\mathbf{p}$ , we find that the P-wave vertex term contributes an S-wave pion emission amplitude that is unfavored by a momentum factor  $p_3^2$ . It is the S-wave vertex term that gives rise to the sought-for amplitude that is independent of external momenta. Such an amplitude is more favorable than P-wave emissions near threshold by two degrees of forbiddenness. It can be expected to dominate the decay width near threshold.

It is true, however, that the S-wave vertex is weaker than the P-wave vertex by a factor  $w/2m$ , and, depending on the dynamical model for  $d'$ , the  $B^*B$  components of  $d'(T=2)$  might themselves be weak. So the quantitative impact of this normal S-wave decay amplitude at the dibaryon mass of 2065 MeV is model-dependent.

Exactly the same situation holds for  $d'(T=0)$  when treated as an S-wave  $N^*N$  bound state, where  $N^*$  is a P-state baryon of isospin 1/2. To the extent that this component might actually be a significant if not major part of  $d'(T=0)$ , the decay width of this dibaryon can be expected to be actually larger than that for  $d'(T=2)$  near threshold.

The qualitative view on the decay of  $d'$  implied by our forbiddenness classification and threshold behaviors both agrees with and differs from those obtained in recent studies of the  $d'$  decay width in interesting ways. For the same models of  $d'$ , we agree with Garcilazo [22] that the

$T=0$  decay width should be larger than the  $T=2$  width, but both our widths are likely to be much smaller than Garcilazo's results. This is because for  $d'(T=0)$ , the normal allowed S-wave decay comes only from the weak S-wave  $\pi qq$  vertex, while for  $d'(T=2)$  without any  $B^*$  component, the  $\ell=2$  forbidden decay width should be relatively small near threshold.

We agree with Obukhovskiy *et al.* [23] in finding that the P-wave  $\pi NN$  vertex causes a recoil-induced decay into S-wave pion and  $NN(^1S_0)$  final state, and that the resulting decay amplitude has an abnormal quadratic dependence on the pion momentum. However, another decay amplitude of comparable importance, namely P-wave pion emission caused by the P-wave  $\pi NN$  vertex and leading to the  $NN(^3P_1)$  final state has not been included in their calculation.

We agree with Samsonov and Schepkin [24] that another problem with the calculation of [23] is that the S-wave  $\pi NN$  vertex has been left out. Its inclusion is important as it gives rise to the dominant allowed S-wave emission near threshold. Much is unclear, however. The energy transfer  $w$  appearing in it is sometimes positive and sometime negative. It is not clear what it averages out to be. It is also not clear how much of the S-wave dominance remains by the time we get to the dibaryon mass of 2065 MeV.

## VII. DISCUSSION AND CONCLUSIONS

Just as in nuclear  $\beta$  decay, a general three-body decay near threshold depends sensitively on the orbital angular momenta of the decay particles in the final state. A classification of the decay widths based on different degrees of  $\ell$ -forbiddenness then becomes useful. Much diversity exists within this broad classification, primarily because some decays are weaker than normal (or are unfavored) due to the presence of additional powers of external momenta in their decay amplitudes.

According to this classification, the decays

$$d^*(J^\pi = 3^+, T=0) \rightarrow \pi(\ell_\pi = 0) NN(^3F_3) \quad \text{and} \quad \pi(\ell_\pi = 1) NN(^1D_2) \quad (63)$$

of the dibaryon  $d^*$  are both normal “third-forbidden” decays. Even among such normal decays, considerable diversity remains in the decay widths due to differences in wave functions and in dynamics.

In this paper, we have used an angle-average approximation to make quick estimates of the  $\pi NN$  decay width of a  $d^*$  described as a simple  $\Delta^2$  bound state. We find a leading-order decay width of only 70 keV at the  $d^*$  mass  $m^*$  of 2100 MeV. The calculated width decreases rapidly as  $m^*$  decreases towards the threshold at 2020 MeV, being only about 6 keV at  $m^* = 2065$  MeV.

The accuracy of these angle-averaged results must be confirmed in the future by more detailed calculation. Such a calculation is conceptually simple, but a little tedious in execution as it involves additional angle integrations. The uncertainties caused by angle averaging are likely to be much smaller than the uncertainties caused by uncertainties in the wave functions and in the strong-interaction dynamics.

Although the  $d^*$  model used here is crude, the calculated results can be used to estimate the decay widths for other models of the wave function. For example, the  $d^*$  wavefunction is much more complicated in the quark-delocalization and color-screening model of [2–4]. It has been estimated [1] that quark delocalization would decrease the present result by a factor of 0.4, while only 1/5 of the six-quark wavefunction is in the  $\Delta^2$  configuration. The remaining 4/5 of the  $d^*$  state is in hidden-color configurations which will contribute much less, perhaps only 1/5 or less of the contribution of  $\Delta^2$ .

The  $d^* \rightarrow NN$  width used here might also have been overestimated by the meson-exchange model used in [1]. This would be the case if the interior of the  $d^*$  dibaryon is a perturbative vacuum where the exchanged mesons do not exist as such and where the dynamics is much weaker. Assuming that the hidden-color contribution is cancelled by the reduction caused by the perturbative vacuum, we are left with a total reduction, for the quark-delocalization and color-screening model of  $d^*$ , of about an order of magnitude from the results reported here for our simple model of  $d^*$  as  $\Delta^2$ .

There are other wave-function uncertainties such as the presence of the  $\Delta^2(^7D_3)$  component, which could be significant or negligible depending on the dynamics assumed to operate at short distances.

We have relied on the familiar meson-exchange model of nuclear forces to generate the dynamics needed in the calculation. Unfortunately, the calculated decay width involves the short-range part of the isovector tensor force where there is much cancellation between the  $\pi$ - and  $\rho$ -exchange contributions. Our knowledge of this particular combination of isovector tensor forces, and of short-distance dynamics in general, seems to be relatively poor.

In spite of these uncertainties, our results seem to suggest that the  $\pi NN$  decay width of  $d^*$  might be too small at low  $d^*$  masses to make it easy to use the few decay pions for particle identification.

## ACKNOWLEDGMENTS

I would like to thank Stan Yen, Terry Goldman, Fan Wang and Gary Love for many helpful discussions and correspondence.

## APPENDIX A: SPIN AVERAGES AND TWO-BODY DECAY AMPLITUDES

The three-body decay  $d^* \rightarrow \pi NN$  involves two groups of two-body reduced matrix elements (RME) – one for  $\pi$  emission from a baryon and one for the two-baryon transition  $BB \rightarrow NN$ , where a baryon could be  $\Delta$  or  $N$ . When brought down to the quark level, the RME's needed for  $\pi$  emission from different baryons are related by the nonrelativistic (NR) quark model as follows:

$$\begin{aligned} (\Delta \| \sigma_1 \tau_1 \| N) &= \frac{8}{3} \sqrt{2}, \\ (\Delta \| \sigma_1 \tau_1 \| \Delta) &= \frac{20}{3}, \quad (N \| \sigma_1 \tau_1 \| N) = \frac{10}{3}. \end{aligned} \quad (A1)$$

where quark 1 is in the baryon.

The operator responsible for the  $BB \rightarrow NN$  transitions needed in Figs. 1a-c is

$$T_{BB} = -(\sigma_1 \times \sigma_4)^{(2)}(\tau_1 \cdot \tau_4), \quad (A2)$$

where quarks 1 and 4 are in two different baryons. The following RME's are needed in our calculations:

$$\begin{aligned} (\Delta^2, ST = 30 \| T_{BB} \| N^2, 10) &= \frac{16}{9} \sqrt{\frac{7}{2}}, \\ (N\Delta, ST = 21 \| T_{BB} \| N^2, 01) &= -\frac{40}{27} \sqrt{5}, \\ (\Delta^2, ST = 21 \| T_{BB} \| N^2, 01) &= \frac{40}{27} \sqrt{2}. \end{aligned} \quad (A3)$$

For comparison, we also give the RME between  $N^2$  states:

$$(N^2, ST = 10 \| T_{BB} \| N^2, 10) = \frac{50}{27} \sqrt{5}. \quad (A4)$$

The spin averages of the product of operator matrix elements appearing in the contributions to the decay width shown in Eq.(12) are relatively easy to calculate directly for the  $d^*$  S-state. For Fig. 1a alone, we have

$$\begin{aligned} &\frac{1}{2S+1} \sum_{M, M_T} \sum_{\mu, m, n} |\langle i | (\sigma_1 \times \sigma_4)_\mu^{(2)} (\tau_1 \cdot \tau_4) \sigma_m \tau_n | f \rangle|^2 \\ &= \frac{25}{24} (\Delta^2, ST = 30 \| T_{BB} \| N^2, 10) (\Delta \| \sigma_1 \tau_1 \| N), \end{aligned} \quad (A5)$$

where

$$\begin{aligned} |i\rangle &= |d^*; S = 3M, T = 00\rangle, \\ |f\rangle &= |(\pi NN) 00, 1M_T\rangle. \end{aligned} \quad (A6)$$

The quark label has been left out of the quark operators  $\sigma_m \tau_n$  responsible for the pion emission. We have also chosen to express this and other spin averages in terms of the RME's for  $\Delta^2 \rightarrow NN$  and  $\Delta \rightarrow \pi N$  for convenience in mutual comparisons. The spin averages for the other

diagrams and for interference terms can be calculated in the same way.

The pion momentum is the same for all Feynman diagrams, but the dependence on the nucleon momenta is more complicated. We shall assume that the  $BB \rightarrow NN$  interaction should be evaluated in the c.m. frame of the baryons in Figs. 1b, c, e and f, and not that of  $d^*$ . This means, for example, that the nucleon momentum appearing in the corresponding decay amplitudes for Figs. 1b and c, denoted  $\mathcal{F}_{2a}$  in the text, is different from that for Fig. 1a, as explained more fully in Sect. II. This refinement is included in the final expression (47), which also gives the results of all spin averages.

Two two-body decay widths (or amplitudes) appear in this equation. The one for the decay  $\Delta \rightarrow \pi N$  is obtained from the free-space decay width  $\Gamma_\Delta$  based on a P-wave  $\pi qq$  vertex for pion emission from quarks. This means that we have neglected a certain well-known S-wave vertex term which when expressed in baryon coordinates is proportional to the mean momentum of the emitting baryon. This S-wave emission vanishes in free space because the appropriate frame to be used is the one where the mean momentum vanishes, i.e. the Breit frame. It does not vanish in a many-baryon system where the mean baryon momentum is nonzero. We have argued in Sec. II, however, that for  $d^*$  decay this S-wave vertex is likely to be much less important than the more familiar P-wave vertex. It may therefore be neglected in the qualitative estimates attempted in this paper.

Two different dynamical inputs for the  $BB \rightarrow NN$  transition amplitudes  $\mathcal{F}_{2a}$  are used in Eq. (47). It depends on the nucleon momentum  $p_2^*$  in the  $B^2$  rest frame of invariant mass  $m_{12}$ :

$$\mathcal{F}_{2a}(p_2^*) = \left( \frac{\sqrt{p_2^* \mu^*}}{2\pi} \right) \sqrt{\frac{8}{15}} \left( \frac{12}{5} \right)^2 \left( \frac{1}{\pi \beta^{*2}} \right)^{3/4} \times e^{-\kappa^2/2} I(\kappa) \left( \frac{\beta^{*5}}{\kappa^3} \right), \quad (\text{A7})$$

where

$$\mu^* = m_{12}/4, \quad \kappa = p_2^*/\beta^*, \quad \beta^* = \sqrt{3/8} r^*, \quad (\text{A8})$$

$r^*$  is the  $d^*$  radius, usually taken to be 0.7 fm, and  $I(\kappa)$  is an integral [1] over the momentum  $q = \beta^* Q$  of the virtual meson responsible for the  $BB$  recoil:

$$I(\kappa) = e^{-\kappa^2/2} \int e^{-Q^2/2} [j_2(i\kappa Q)(\kappa Q)^3] t_{\text{ivt}}(\beta^* Q) Q dQ. \quad (\text{A9})$$

The function  $t_{\text{ivt}}(q)$  is the radial part of the isovector tensor force appearing in both meson- $qq$  and meson- $BB$  interactions.

For the Full-Bonn (FB) potential [5] in the Born approximation, we use

$$t_{\text{ivt}}(q) \approx v_{\text{ivt}}(q) = \sum_i v_i(q), \quad (\text{A10})$$

where

$$v_i(q) = 4\pi \frac{S_i \alpha_i}{4m_i^2 q^2 + m_i^2} \left( \frac{\Lambda_i^2 - m_i^2}{\Lambda_i^2 + q^2} \right)^2. \quad (\text{A11})$$

The sum is taken over the two virtual mesons  $i = \pi, \rho$ , with signatures  $S_\pi = -1, S_\rho = 1$  and strengths

$$\alpha_\pi = \frac{g_\pi}{4\pi} = 14.4, \quad \alpha_\rho = \frac{g_\rho^2}{4\pi} \left( 1 + \frac{f_v}{g_v} \right)^2 = 0.84(1 + 6.1)^2, \quad (\text{A12})$$

respectively. The other parameters are those shown on p. 37 of [5].

For the Love-Franey  $t$ -matrix, we use Eq. (15c) of [25]

$$t_{\text{ivt}}(q) = \sum_i t_i(q), \quad (\text{A13})$$

where

$$t_i(q) = 32\pi \frac{V_i^T q^2 R_i^7}{[1 + (qR_i)^2]^3}. \quad (\text{A14})$$

This is a sum of 3–4 terms of different ranges  $R_i$  corresponding to virtual mesons of different masses  $m_i = \hbar c/R_i$ . The parameters are given in Table I of [6].

In the approximation described in Sec. V, two of the retardation amplitudes  $\mathcal{R}$  involve the same function:

$$\mathcal{R}_{2d}(f; p_2^*) = \mathcal{R}_{2d}(d; p_2^*). \quad (\text{A15})$$

Only two distinct functions are then needed. Both are generated from Eq. (A7), but by using a certain retardation analogs  $r_{\text{ivt}}$  of  $t_{\text{ivt}}$ . For the FB potential, they are

$$r_{\text{ivt}}(\alpha; q) = \sum_i \frac{v_i(q) \omega_i}{D_{0i} D_{\alpha i}}, \quad (\text{A16})$$

where the argument  $\alpha = d$  ( $e$ ) denotes Fig. 1d (1e),  $\omega_i = \sqrt{m_i^2 + q^2}$ , and

$$D_{0i} \approx m^* - \omega_i - \langle E_2 \rangle - \langle E_\Delta \rangle, \quad D_{\alpha i} \approx \langle E_2 \rangle - \omega_i - \langle E_B \rangle. \quad (\text{A17})$$

The baryon energy  $E_B$  is  $E_\Delta$  for  $\alpha = d$ , and the nucleon energy  $E$  for  $\alpha = e$ . The averages appearing here are those described in Sec. V.

For the LF  $t$ -matrices, the Born term  $v_i$  in Eq. (A16) should be replaced by the  $t$ -matrix term  $t_i$ .

---

[1] C.W. Wong, Phys. Rev. C **57**, 1962 (1998).

- [2] T. Goldman, K. Maltman, G.T. Stephenson, Jr., K.E. Schmidt, and F. Wang, Phys. Rev. C **39**, 1889 (1989); F. Wang, J.L. Ping, G.H. Wu, L.J. Teng, and T. Goldman, *ibid* **51**, 3411 (1995).
- [3] F. Wang, G.H. Wu, L.J. Teng, and T. Goldman, Phys. Rev. Lett. **69**, 2901 (1992).
- [4] T. Goldman, K. Maltman, G.T. Stephenson, Jr., J.L. Ping, and F. Wang, "Systematic Theoretical Search for Dibaryons in a Relativistic Model", Los Alamos Report LA-UR-95-2609.
- [5] R. Machleidt, K. Holinde, and Ch. Elster, Phys. Rep., Phys. Lett. **149C**, 1 (1987).
- [6] M.A. Franey and W.G. Love, Phys. Rev. C **31**, 488 (1985).
- [7] H. Sugarwara and F. von Hippel, Phys. Rev. **185**, 2046 (1969).
- [8] T. Ericson and W. Weise, *Pions and Nuclei* (Clarendon Press, Oxford, 1988), p120.
- [9] T.-S. H. Lee and D.O. Riska, Phys. Rev. Lett. **70**, 2237 (1993).
- [10] C. Hanhart, J. Haidenbauer, A. Reuber, C. Schütz, and J. Speth, Phys. Lett. B **358**, 21 (1995).
- [11] H.T. Coelho, T.K. Das, and M.R. Robilotta, Phys. Rev. C **28**, 1812 (1983).
- [12] Particle Data Group, *Review of Particle Physics*, Phys. Rev. D **54**, 1 (1996).
- [13] G. Källen, *Elementary Particle Physics* (Addison-Wesley, Reading, MA, 1964), pp. 193-199.
- [14] G.E. Brown and W. Weise, Phys. Rep., Phys. Lett. **22C**, 279 (1975).
- [15] V.R. Brown, Phys. Rev. **177**, 1498 (1968).
- [16] V. Herrmann and K. Nakayama, Phys. Rev. C **46**, 2199 (1992); F. de Jong and K. Nakayama, Phys. Lett. B **385**, 33 (1996).
- [17] J.A. Eden and M.F. Gari, Phys. Rev. C **53**, 1102 (1996).
- [18] R.A. Arndt, L.D. Roper, R.A. Bryan, R.B. Clark, B.J. VerWest, and P. Signell, Phys. Rev. D **28**, 97 (1983); R.A. Arndt and L.D. Roper (unpublished); R.A. Arndt, private communication via G. Love.
- [19] R. Bilger *et al.*, Z. Phys. **A343**, 491 (1992); R. Bilger, H.A. Clement, and M.G. Schepkin, Phys. Rev. Lett. **71**, 42 (1993); **72**, 2972 (1994).
- [20] L.S. Vorobev *et al.*, JETP Lett. **59**, 77 (1994).
- [21] W. Brodowski *et al.*, Z. Phys. A **355**, 5 (1996).
- [22] H. Garcilazo, J. Phys. G **23**, 1101 (1997).
- [23] I.T. Obukhovsky, K. Itonaga, Georg Wagner, A.J. Buchmann, and Amand Faessler, Phys. Rev. C **56**, 3295 (1997).
- [24] A. Samsonov and M. Schepkin, Los Alamos Eprint nucl-th/9712079.
- [25] W.G. Love and M.A. Franey, Phys. Rev. C **24**, 1073 (1981).

### Figure Captions

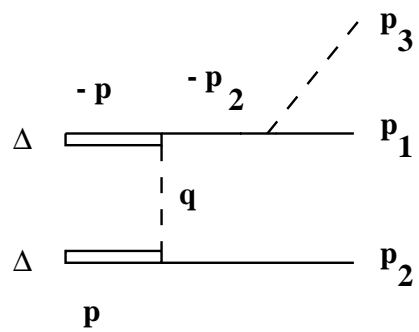
FIG. 1. Some leading-order Feynman diagrams for the decay  $d^* \rightarrow \pi NN$  with pion emission from a baryon.

FIG. 2. Some leading-order Feynman diagrams for the decay  $d^* \rightarrow \pi NN$  with pion emission from virtual mesons.

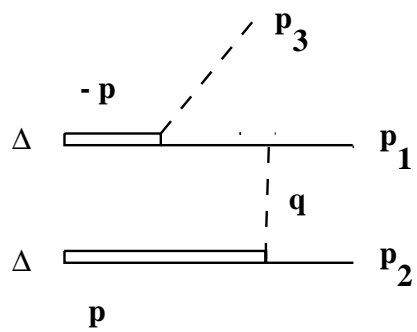
FIG. 3. The  $d^* \rightarrow NN$  decay width parameter  $\Gamma_{2a}(p)/p^2$  as a function of the off-shell nucleon momentum  $p$  in the  $NN$  c.m. frame for the Full Bonn (FB) and the Love-Franey (LF) models of dynamics. Each LF curve is labeled by the c.m. energy of the  $NN$  system whose empirical free-space  $t$ -matrix is used in the calculation. The on-shell decay width at each energy is given by a solid circle in the figure.

FIG. 4. The widths  $\Gamma_a$  from Fig. 1a alone and  $\Gamma_{ac}$  from Figs. 1a-c for the decay  $d^* \rightarrow \pi NN$  for different dynamical inputs: the Full Bonn potential (FB), Love-Franey  $t$ -matrices calculated at the dibaryon energy (LF-DBE) and at the  $NN$  energy (LF-NNE).

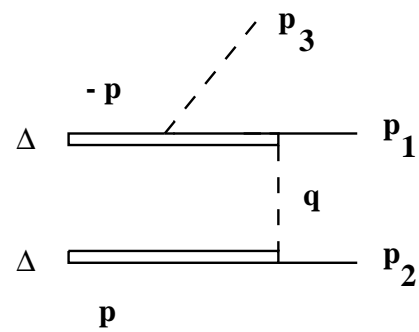
FIG. 5. Ratios of the Dalitz area  $A$ , the decay width  $\Gamma_a$  from Fig. 1a, and the decay width  $\Gamma_{af}$  from Figs. 1a-f to the expected threshold power law for the  $d^* \rightarrow \pi NN$  decay as functions of the dibaryon mass  $m^*$ . Each ratio is given in units of the value at  $m^* = 2034$  MeV.



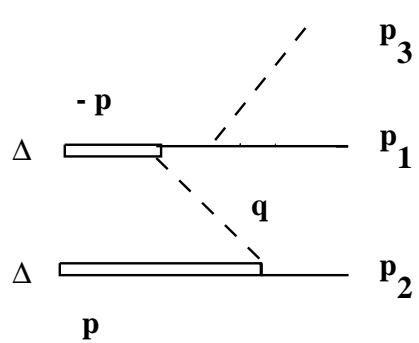
(a)



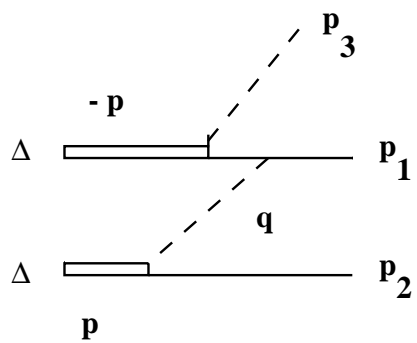
(b)



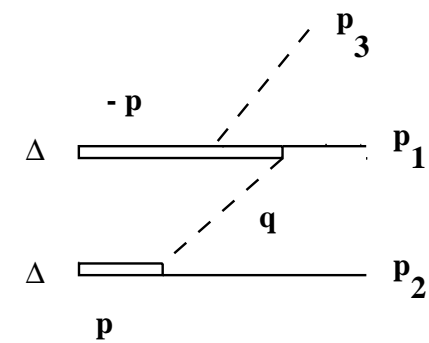
(c)



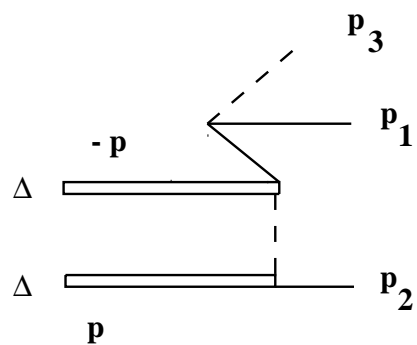
(d)



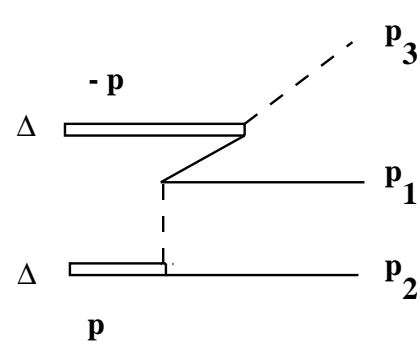
(e)



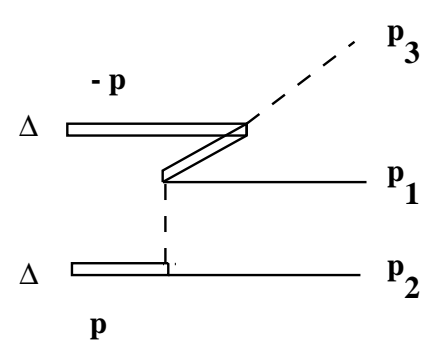
(f)



(g)



(h)



(i)



